Projectile energy loss in multiply ionizing ion-atom collisions

H. Schöne,[1,*] R. Schuch,[2] S. Datz,[1] M. Schulz,[1,†] P. F. Dittner,[1] J. P. Giese,[1,‡] Q. C. Kessel,[3] H. F. Krause,[1] P. D. Miller,[1] and C. R. Vane[1]

[1]*Physics Division, Oak Ridge National Laboratory, P.O. Box 2008, Oak Ridge, Tennessee 37831-6377*

[2]*Atomic Physics, Stockholm University, Frescativagen 24, S-104 05 Stockholm 50, Sweden*

[3]*Department of Physics, University of Connecticut, Storrs, Connecticut 06268*

(Received 9 May 1994)

The projectile energy loss for 7.5–25-MeV $C^{6+,5+}$ and F^{6+} ions was measured for single collisions with He, Ne, Ar, and Kr as a function of the recoil-ion charge state and the projectile scattering. This energy loss was measured for collisions in which the projectile captured an electron and for those involving just direct ionization. We investigated and found a large average energy transfer (100–250 eV/electron) to the continuum electrons. A strong increase of the scattering angle with recoil-ion charge state was observed for both capture and direct ionization. The results imply that, for smaller impact parameters, higher recoil-ion charge states are produced and that higher energy losses are obtained. We observed a weak target-Z dependence of the energy loss. The results are compared with n-body classical-trajectory Monte Carlo calculations by Olson, semiclassical-approximation calculations by Schuch *et al.* [Nucl. Instrum. Methods Phys. Res. Sect. B **42**, 566 (1989)], and the energy-deposition model.

PACS number(s): 34.50.Fa, 34.70.+e

I. INTRODUCTION

Inelastic collisions between heavy ions and target atoms are governed by complex interaction dynamics where excitation, ionization, and charge transfer are possible. Collective interactions of the nuclei and all the electrons may also open new reaction channels. Over the last few years there has been a strong effort to understand the fundamental dynamics involved in such many-particle systems. Collective effects may also be important, as in multiple ionization, and these have been studied extensively via, e.g., electron spectroscopy, recoil-ion time of flight, and recoil energy spectroscopy. Exact solutions, however, are not possible even for the simplest of n-particle problems. Nevertheless, measured total ionization cross sections [1–3] are generally well described by the independent-particle model (IPM) [4]. The IPM excludes all electron-electron interactions that go beyond an effective screening potential such as Thomas-Fermi potential or energetically correct wave functions such as Hartree-Fock. The calculation of the projectile's trajectory is generally simplified by assuming a two-body collision between projectile and target nuclei. Again the electrons are accounted for by an effective screening potential. This only permits the computation of single electron ionization probabilities [5–7] and application of binomial statistics to obtain the multiple ionization cross sections [6–9]. In addition, the IPM is useful in predicting the recoil-ion charge-state distribution for targets with more than one electron shell involved in the ionization when Auger cascades are taken into account [10–13]. Stringent tests of the existing models with experiments involving recoil-ion production cross-section measurements that are either differential in projectile exit charge state and scattering angle [14–17], or in the projectile's scattering angle and electron energy have been conducted [18,19]. These experiments indicate derivations from the IPM, which are believed to originate from the exclusion of dynamic effects, such as time-dependent screening, which occur during the collision.

Recoil-ion production cross sections peaking in backward angles have been observed for low recoil-ion charge states. At first glance this appears surprising. For impact parameters larger than the atomic radius, the transverse momentum transferred to electrons and recoils is, according to the impulse approximation, only governed by the Coulomb interaction and is, therefore, the same for both. In contrast, the energy transferred to either one will differ notably by the mass ratio and the square of the recoil charge, i.e., $E_e/E_r=(m_e/M_r)Z_r^2$. In order to observe backward recoil scattering angles in these instances, the ejected electrons have to carry a considerable momentum out of the collision. The n-body classical-trajectory Monte Carlo (nCTMC) calculation for the collision system of 1.4 MeV/amu $U^{32+}+Ne$ presented in Olson, Ullrich, and Schmidt-Böcking [17] provides a possible insight into the collision dynamics. The authors calculated the scattering yields for electrons, recoils, and projectiles in the azimuthal plane perpendicular to the initial direction of the projectile. The results indicate that for low-recoil charges states $q \leq 4$, the electrons are preferentially emitted toward the plane spanned by the projectile path and recoil position. The projectile is scattered to negative

*Present address: Sandia National Laboratory, Department 1111, Albuquerque, NM 87185.

†Present address: Department of Physics, University of Missouri, Rolla, MO 65401.

‡Present address: Department of Physics, Kansas State University, Manhattan, KS 66505.

deflection angles mainly due to the anisotropically emitted electrons. Their position between projectile and target will not only screen the target potential but actually attract the projectile. Secondly, and to a lesser degree significant, the projectile will be influenced by the dipole polarization of the target by the projectile's potential. Only for large recoil charge states $q \geq 7$ is the projectile-recoil nucleus interaction dominating the scattering. These calculations are supported by recoil transverse energy measurements [14,15,20]. Hence, a simple two-body collision between the projectile and target nucleus cannot be assumed to give a good approximation of the impact parameter from a determination of the projectile's scattering angle. Highly differential measurements such as those reported in this paper are necessary for a detailed understanding of the collision dynamics. Previously, we have reported measurements of inelasticities for 10-MeV C projectiles colliding with Ne [21]. In this paper, we report on the energy loss of 7.5–25-MeV C and F projectiles in He, Ne, Ar, and Kr gases. The measured energy losses accompanying direct ionization or capture plus multiple ionization are an important control parameter for collision dynamics because they give the sum of all target electron removal processes with their associated inelastic energies. This makes it possible to estimate the importance of collective effects, such as polarization, during ionization.

II. EXPERIMENTAL SETUP

The experiments were performed at the EN Tandem of the Oak Ridge National Laboratory. Figure 1 shows the experimental setup used. The primary ion beam was energy and charge-state selected with the first 90° magnet before post stripping. A second 90° magnet in conjunction with two energy defining slits ($S1$ and $S2$) selected the final charge state and set the conditions for a high-energy resolution. After traversing the gas target region, the ion's energy loss and scattering angle were determined in a high-resolution Elbek-type magnetic spectrometer [22]. The Elbek spectrometer is second-order focusing in the plane of dispersion and nonfocusing in the perpendicular plane. The ions were detected with a two-dimensional, chevron-type channel-plate detector assembly located in the focal plane of the spectrometer. In order to obtain the maximum energy resolution of the spectrometer ($\Delta E/E = 10^{-4}$ and $\Delta p/p = 3 \times 10^{-5}$, respectively) and good scattering angle resolution, the projectile beam was collimated to 0.1 mm × 0.1 mm ($\leq 3 \times 10^{-2}$ mrad) before entering the target region. The contribution of the fringing fields to the beam distortion was minimized by choosing the largest possible bending radius. Due to the second-order focusing properties in the plane of dispersion of the spectrometer, an exact scattering angle dependent intensity distribution can only be obtained after deconvoluting [21,23] the experimental distribution. However, the appropriate corrections are small and not critical to the interpretations made. These corrections are therefore neglected in the reported spectra. Because of the large dispersion, only one charge state struck the detector. The other charge states were either collected in a Faraday cup or struck the spectrometer walls.

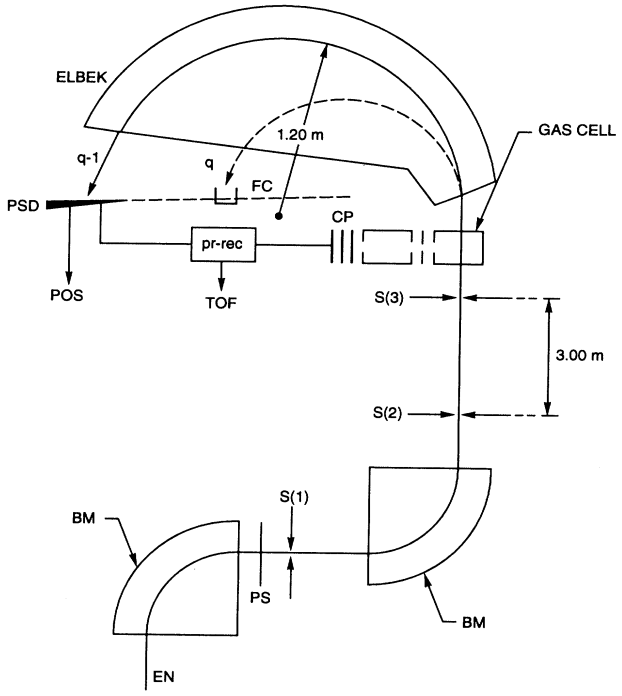

FIG. 1. Schematic of experimental setup used. Parts are designated as: EN, EN Tandem Van de Graaf Accelerator; BM, bending magnets; PS, post stripper foils; $S(1)$, $S(2)$, and $S(3)$, four-jaw slits 1–3; FC, Faraday cup; PSD, position sensitive detector; pr-rec, projectile-recoil coincidence electronics; TOF, time-of-flight measurement; and CP, recoil ion detector.

An electrostatic field, within the target region, extracted recoil ions at 90° with respect to the beam axis. A time-of-flight measurement between recoils and projectiles allowed us to associate the projectile energy loss with the recoil charge state produced. The design of the gas cell and the recoil time-of-flight spectrometer are shown in Fig. 2.

We deal with two cases: direct target ionization with no capture designated DI and target ionization accompanied by capture onto the projectile designated cap. In the case of direction ionization (DI) with no charge change, an absolute energy loss with respect to the primary beam energy could be established by observing the position of the unscattered beam on the detector. In the case where the projectile has changed charge (cap) this is not possible, since the absolute energy of the beam cannot be measured with sufficient accuracy ($\Delta E/E \sim 10^{-6}$). The energy loss in cap experiments is determined relative to the arbitrary reference point of singly charged recoil ions. Energy calibration of a position displacement on the projectile detector was achieved [24] by biasing the gas cell to a well defined voltage (e.g., +5 kV). Projectiles that captured an electron outside the gas cell will not be affected by the gas cell potential, while those that captured an electron inside the gas cell to form an ion of charge $q-1$ will have 5-keV less energy. A schematic diagram of the experimental setup and resulting position

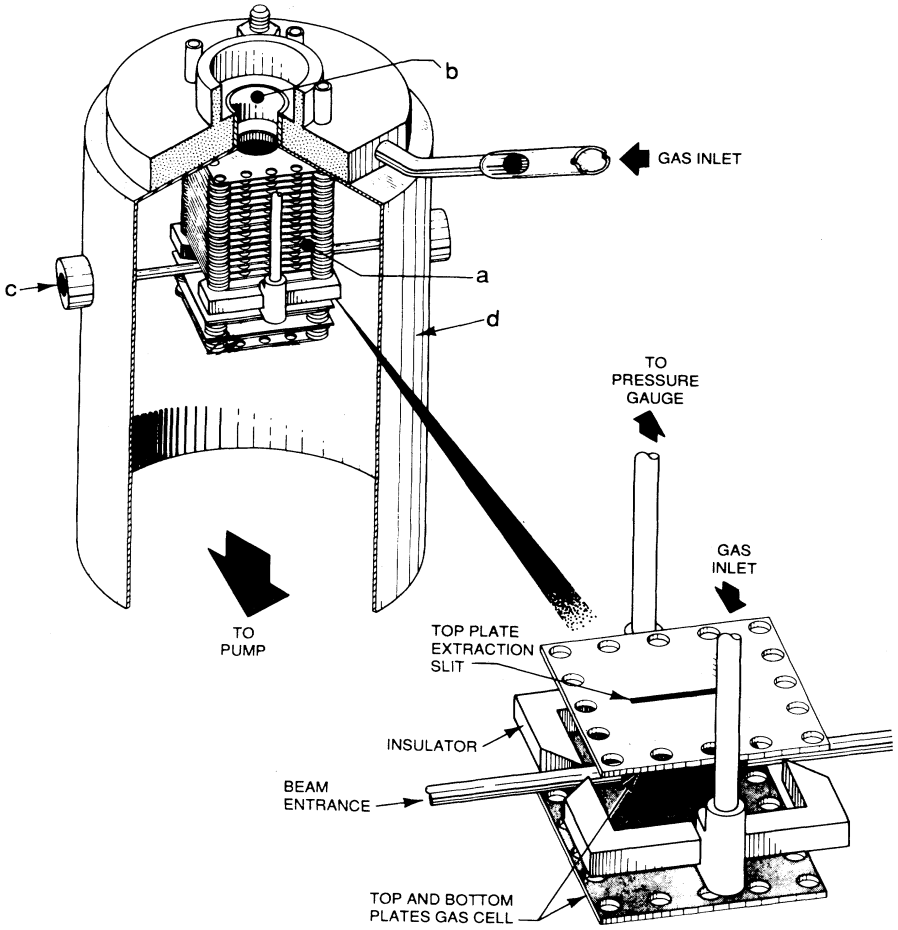

FIG. 2. Drawing of gas cell and recoil time-of-flight spectrometer. (a) Gas cell and recoil acceleration region; (b) recoil drift region (channel plate detector not shown); (c) beam entrance aperture diameter 1 mm; and (d) first differential pumping stage. Also shown is an exploded view of the gas cell.

distribution on the projectile detector projected on the axis of dispersion is shown in Fig. 3. Uncertainties in determining the peak positions and the gas cell bias voltage results in an absolute error in the energy calibration of ± 5 eV.

III. EXPERIMENTAL DATA

In this section, we illustrate the data extraction for some typical collision systems. Windows set on the different charge states allowed us to differentiate the projectile position distribution in coincidence with a given recoil charge state. The resulting distributions are shown in Fig. 4 for the case C^{6+} (10 MeV)$+Ne \rightarrow C^{6+}+Ne^{q+}+qe^{-}$ and Fig. 5 for the case C^{6+} (10 MeV) $+Ne \rightarrow C^{5+}+Ne^{q+}+(q-1)e^{-}$. In these figures, the projectile distribution moves to successively larger inelasticities with increasing target ionization and the distributions widen in the scattering angle (y) plane. The dashed line in Fig. 5 indicates the location of the centroid of the Ne^{1+} distribution and served as an arbitrary reference point for the energy shift. To the left of the main distribution, background events resulting from direction ionization of the target and capture outside the target region are seen. Even though the energy loss increases for larger recoil charge states, there is for a given recoil charge state (within our resolution of ± 50 eV) no

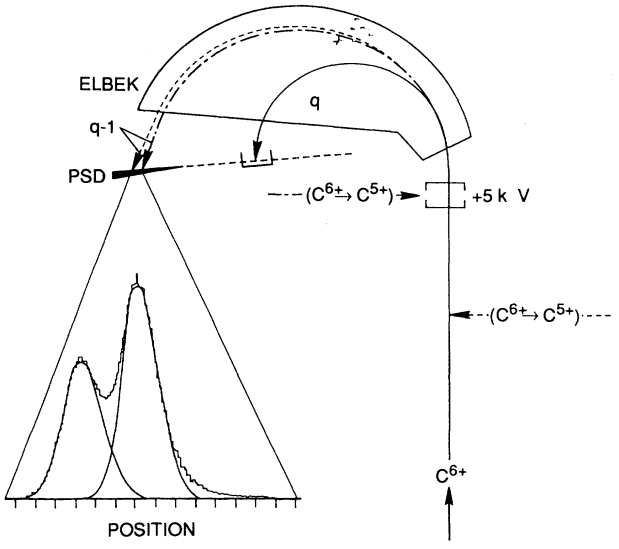

FIG. 3. Energy calibration. Projectiles that charge capture within the biased gas cell (dashed line) will be decelerated by 5 keV and projectiles that capture an electron outside the target ell (dash-doted line) will not be affected by the bias voltage. The resulting position distribution along the plane of dispersion is also shown. Projectiles that do not capture are collected in a Faraday cup.

correlation between energy loss and scattering angle in the y direction. Since the beam is focused in momentum in the x direction, what we observe is a projection of the true angular distribution on the y axis. Thus, if the formation of, e.g., Ne^{6+} were to take place in a limited region of impact parameter, the angular distribution associated with Ne^{6+} would be doughnut shaped and its projection would be as in Figs. 4 and 5. The small rotation of the $2d$ distributions in Figs. 4 and 5 was verified to be an artifact of our experimental setup and does not represent any physical process. Energy loss was determined by projecting the two-dimensional (2D) distribution on the plane of dispersion (see Fig. 6). Because of the independence of the energy loss from the scattering angle in the x-y plane, the projection did not introduce any additional errors. The energy loss for producing a given recoil charge state was determined by finding the centroid of each distribution.

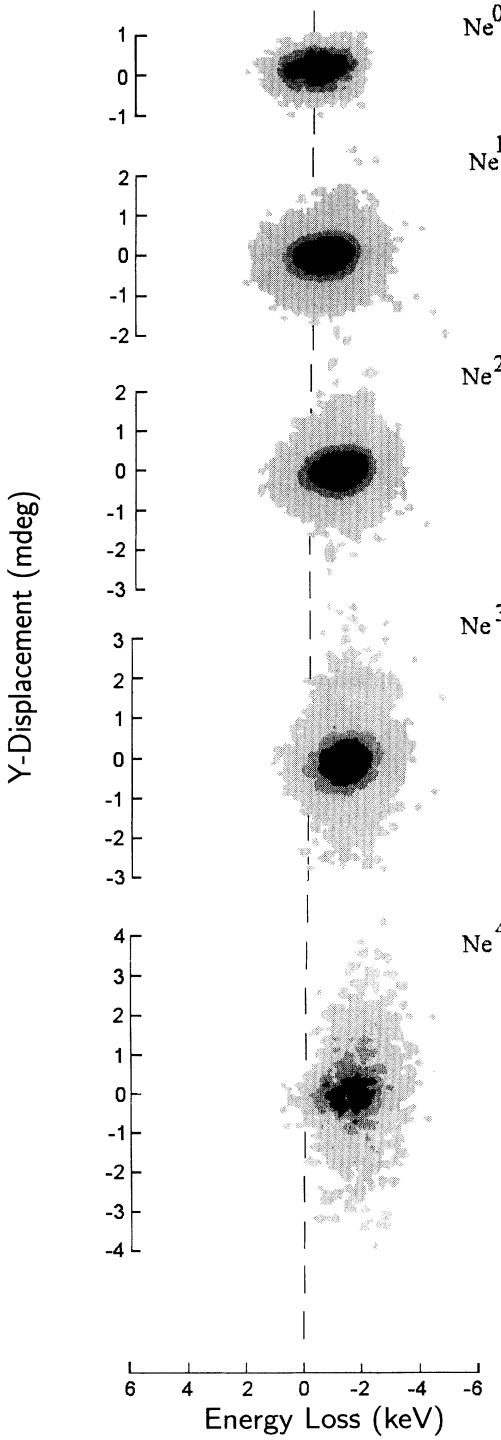

FIG. 4. Two-dimensional contour plot of projectile ion distributions in coincidence with recoil-ion charge state for direction ionization, i.e., $C^{6+}+Ne \rightarrow C^{6+}+Ne^{q+}+qe^{-}$. Ne^{0+} represents the projectile that did not ionize any target electrons.

IV. DATA REDUCTION

Although typical base pressures along beam lines were better than 5×10^{-8} Torr and 2×10^{-7} Torr with a typical target gas pressure of 1 mTorr, double collision in the gas cell and contributions of charge exchange from residual gas with a subsequent target collision (or vice-versa) could lead to false coincidences and hence false energy losses. A clean-up magnet could not be used in this experiment since it would have compromised the beam quality. Instead, we biased the gas cell during data acquisition and were able to identify background events. However, double collisions within the gas cell were present since some differential cross sections investigated were too small to permit the further reduction of the target gas pressure, which would be required to ensure single collision conditions. Contributions from double collisions were only significant for projectile charge capture in coincidence with singly or doubly ionized recoil ions. Contributions from these background events are noticeable in Fig. 5 as weak beam spots to the left of the main distribution. They are most pronounce for recoil charge-state one and decrease as the DI cross sections for higher charge states. The maximum contribution of double collisions can be estimated as follows. For capture to the projectile and multiple ionization of the target (to a final charge state of q), we can write the number of true coincidences N^{q+}_{true} as

$$N^{q+}_{\text{true}} = N_0 \sigma^{q+}_{\text{cap}} nl \epsilon_{\text{rec}} \epsilon_{\text{pr}} , \tag{1}$$

where N_0 is the number of incoming projectiles, σ^{q+}_{cap} is the cross section for single capture and the formation of recoil ions with charge q, nl is the target thickness, and ϵ_{rec} and ϵ_{pr} are the recoil and projectile detection efficiency, respectively. The number of coincidence produced in double collisions N^{q+}_{dou} within the gas target is given by

$$N^{q+}_{\text{dou}} = N^{\text{tot}}_{\text{cap}} \sigma^{q+}_{\text{DI}} nl \epsilon_{\text{rec}} \epsilon_{\text{pr}} , \tag{2}$$

where σ^{q+}_{DI} is the cross section for directly ionizing the target q times and $N^{\text{tot}}_{\text{cap}}$ is the number of projectiles that captured an electron and produced a recoil ion of arbitrary charge state, i.e.,

$$N^{\text{tot}}_{\text{cap}} = N_0 \sigma^{\text{tot}}_{\text{cap}} nl (1-\epsilon_{\text{rec}}) , \tag{3}$$

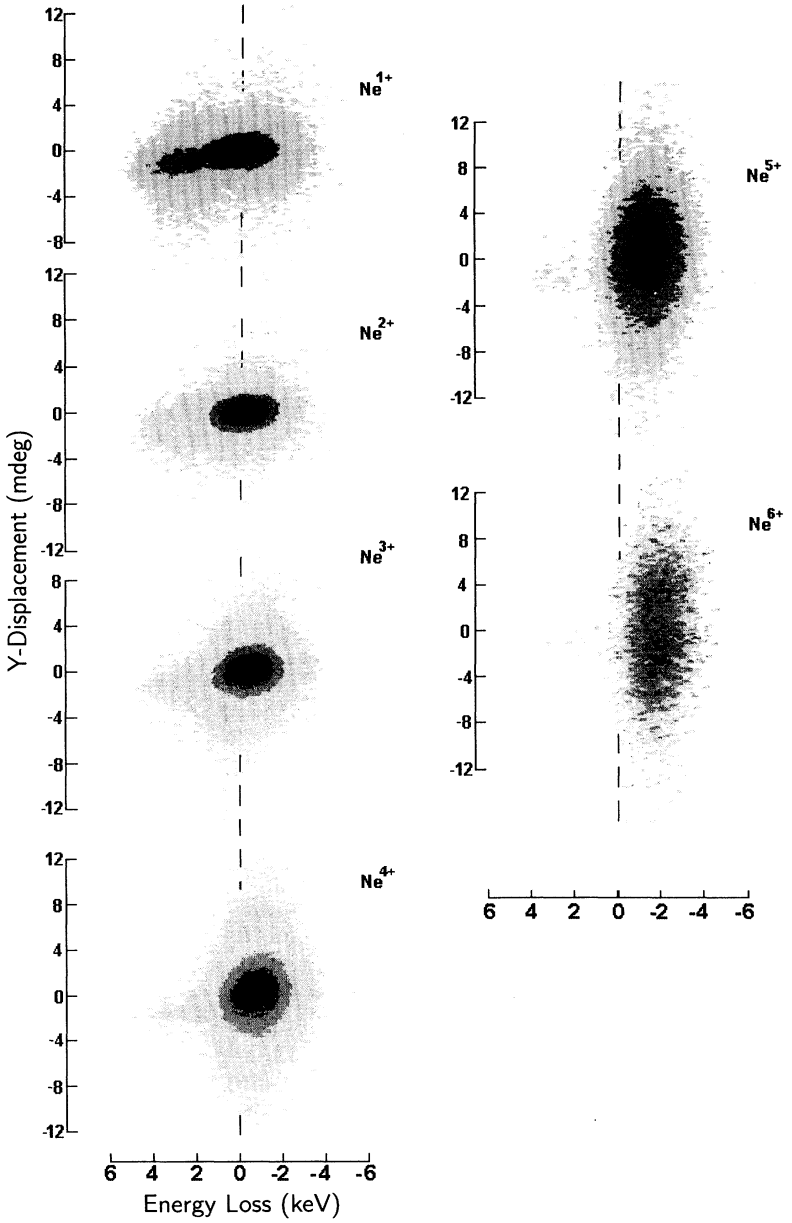

FIG. 5. Two-dimensional contour plot of projectile ion distributions in coincidence with recoil-ion charge state for collisions involving electron capture to the projectile, i.e., $C^{6+}+Ne \rightarrow C^{5+}+Ne^{q+}+(q-1)e^-$.

where σ_{cap}^{tot} is the total cross section. From Eqs. (1), (2), and (3), it follows that

$$\frac{N_{dou}^{q+}}{N_{cap}^{q+}} = \frac{\sigma_{cap}^{tot}\sigma_{DI}^{q+} nl(1-\epsilon_{rec})}{\sigma_{cap}^{q+}} . \quad (4)$$

Table I lists the necessary corrections made to the measured capture cross sections for the example of 10-MeV $C^{6+}+X \rightarrow C^{5+}+X^{q+}$ according to Eq. (4). For all other recoil charge states, the contribution from double collisions is negligible. The energy loss associated with the double collision correction ΔE_{dou}^{q+} is the sum of the energy required to ionize the target q times and the average energy required to capture an electron and accelerate it up to projectile energy, thus

$$\Delta E_{dou}^{q+} = \Delta E_{DI}^{q+} + \sum_{q=1}^{q=5} \Delta E_{cap}^{q+} \frac{\sigma_{cap}^{q+}}{\sigma_{cap}^{tot}} . \quad (5)$$

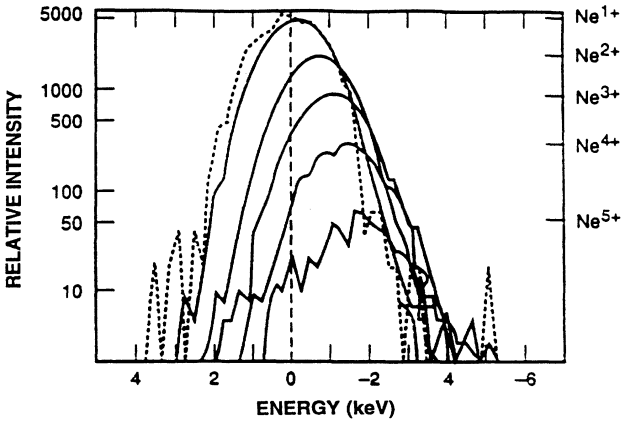

FIG. 6. Projection of position distribution onto axis of dispersion. Dashed line depicts the open ion beam.

TABLE I. Corrections of measured capture cross sections (cm^2) for double collisions according to Eq. (4). σ_{cap}^{tot}, taken from Knudsen [33] measured σ_{cap}^{q+}, is normalized to σ_{cap}^{tot}. σ_{DI}^{q+} measured ionization cross section. The numbers in brackets denote multiplicative powers of ten.

Target	σ_{cap}^{tot}	σ_{DI}^{q+}	σ_{cap}^{q+}	σ_{dou}^{q+}	Error (%)
He^{1+}	4[−18]	8.3[−16]	2[−18]	1[−19]	5
Ne^{1+}	2.6[−17]	3[−16]	2.9[−18]	3.7[−19]	13.3
Ar^{1+}	3.3[−17]	2.3[−15]	1.5[−18]	4.8[−19]	32
Ar^{2+}	3.3[−17]	6.6[−15]	1.3[−18]	1.8[−19]	14.4
Ar^{3+}	3.3[−17]	2.3[−16]	2.7[−18]	4.3[−20]	6
Kr^{1+}	1[−16]	2.8[−15]	2[−18]	1.6[−18]	80
Kr^{2+}	1[−16]	1[−15]	1.3[−18]	4.8[−19]	37
Kr^{3+}	1[−16]	3.9[−16]	3.2[−18]	2[−19]	6
Kr^{4+}	1[−16]	1.5[−16]	9.5[−18]	9[−20]	0.95

V. RESULTS

A. Direct ionization

In Fig. 7, we have plotted the absolute projectile energy loss of 10-MeV C^{6+} ions as a function of the recoil charge state for various target gases. The projectile energy loss increases almost linearly with the number of electrons liberated from the target. After subtracting the sum of the ionization energies required to attain a given charge state (see Table II) [25], the average energy lost by the projectile per ionized electron is on the order of 200 eV. According to the arguments made earlier [21,24] that the recoil-ion energy and target excitation energy are negligible, it is reasonable to assume that all the projectile's energy loss is transferred to the ejected electrons. This implies that on the average, we transfer a constant amount of energy to the continuum electrons, regardless of the final ionization stage of the target.

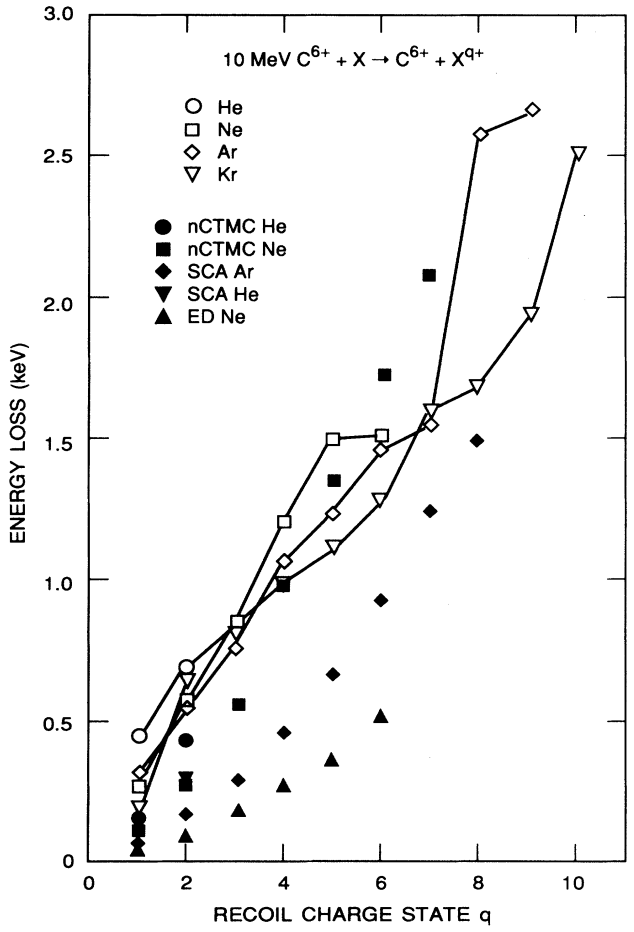

FIG. 7. Absolute projectile energy loss for 10-MeV C^{6+} directly ionizing He, Ne, Ar, and Kr. Included are SCA energy-loss calculations for He and Ar, *n*CTMC calculations for He and Ne, and an energy-deposition model calculation.

Included in Fig. 7 are energy-loss calculations by Olson [26] for He and Ne and calculations by Schuch *et al.* [27] for He and Ar. As can be seen, the semiclassical-approximation (SCA) calculation by Schuch *et al.* greatly underestimates the energy loss, in particular the energy loss for low-recoil charge states. Furthermore, the calculated energy loss increases more than linearly, which suggests that the energy of the electrons ejected increases strongly with the degree of target ionization in contradiction to our findings. While the energy deposition model [28] can give a reasonable account of measured recoil charge-state distributions [1,23], it does not do as well as the calculations mentioned above in accounting for the

TABLE II. Sum of ionization energies (in eV) required to obtain a given charge state [24].

Charge state	He	Ne	Ar	Kr
1+	24.6	21.6	15.8	14.0
2+	79.0	62.6	43.4	38.4
3+		127.1	84.1	75.3
4+		224.2	143.9	127.8
5+		250.4	218.9	192.5
6+		508.3	309.9	271.0
7+			434.2	382.0
8+			577.5	507.9
9+			1000.0	738.8
10+			1479.7	1007
11+				1325
12+				1692

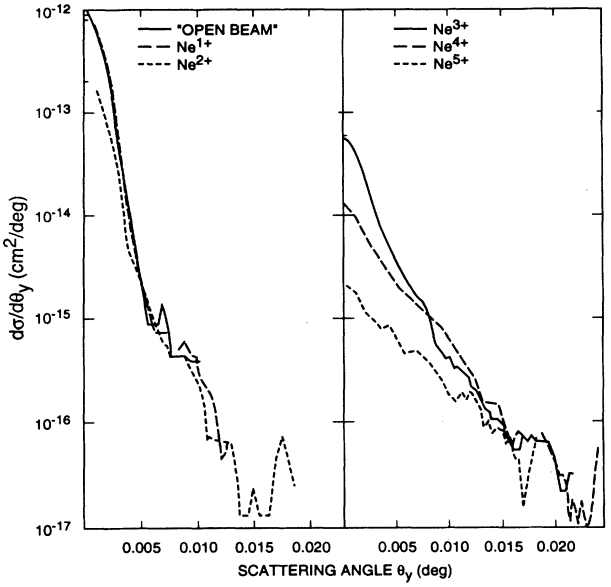

FIG. 8. Differential cross section and projection of angular distribution in the x-y plane for 10-MeV C^{6+} ions in coincidence with Ne^{q+}. "Open beam" depicts the beam profile not altered by target interactions.

observed large energy loss. This statistical model is based on the restrictive boundary condition that all valence electrons initially share the same binding energy. In particular, the model greatly underestimates the energy transfer for higher recoil charge states.

The distribution of ions in the vertical direction of the two-dimensional position-sensitive detector (2DPSD) gives a projection of the launch angle cone onto the x-y

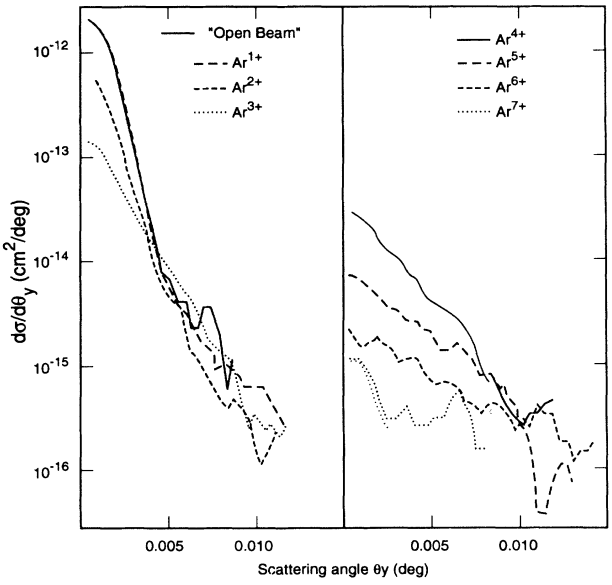

FIG. 9. Differential cross section and projection of angular distribution in the x-y plane for 10-MeV C^{6+} ions in coincidence with Ar^{q+}. "Open beam" depicts the beam profile not altered by target interactions.

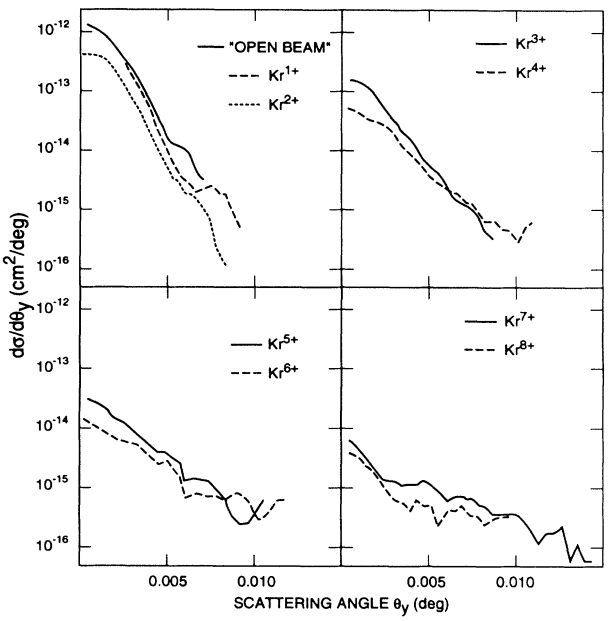

FIG. 10. Differential cross section and projection of angular distribution in the x-y plane for 10-MeV C^{6+} ions in coincidence with Kr^{q+}. "Open beam" depicts the beam profile not altered by target interactions.

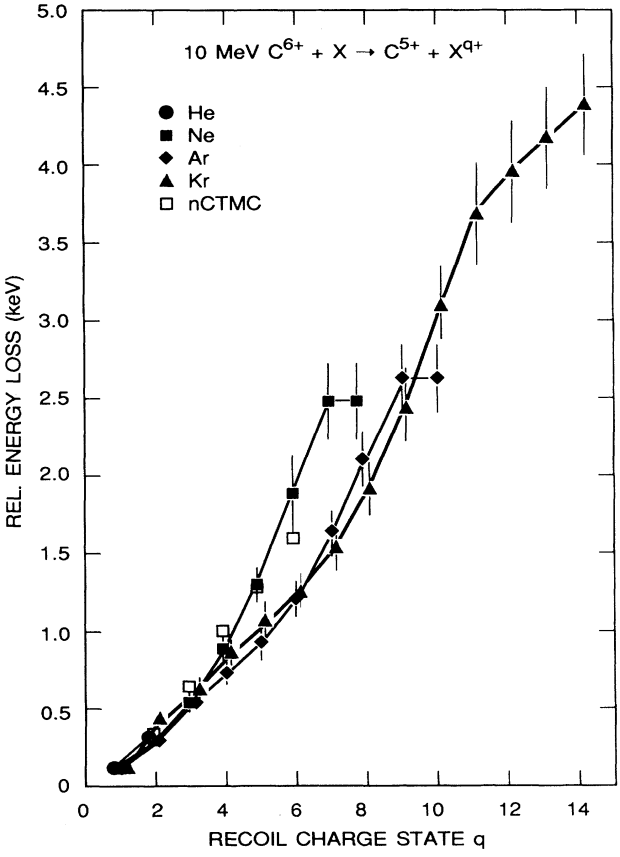

FIG. 11. Relative projectile energy loss for 10-MeV C^{6+} capturing one electron and multiply ionizing He, Ne, Ar, and Kr. The nCTMC calculations were done by Olson [26]. Only systematical error bars are shown. Statistical errors are negligible.

TABLE III. Target and projectile 10-MeV C^{6+} n-state-dependent OBK approximation for single charge transfer cross sections as percentage of the total transfer cross section. Energies in eV represent the binding energy balance between target and projectile minus the acceleration energy of the captured electron ($E_{kin}=456$ eV). Negative signals correspond to a net energy loss of the projectile.

Target gas	C ($n=1$)	C ($n=2$)	C ($n=3$)
He ($n=1$)	4.3% (+10 eV)	42.1% (−357 eV)	33.4% (−425 eV)
Ne ($n=1$)	1% (−830 eV)	<0.6% (−1080 eV)	<0.15% (−1270 eV)
Ne ($n=2$)	39.6% (~0 eV)	32.5% (−360 eV)	11.9% (−430 eV)
Ar ($n=2$)	19.2% (−200 eV)	1.3% (−570 eV)	0.3% (−600 eV)
Ar ($n=3$)	54.8% (+20 eV)	18.6% (−345 eV)	5.7% (−414 eV)
Kr ($n=3$)	6.1% (−54 to −183 eV)	<0.01%	<0.01%
Kr ($n=4$)	86.4% (10 to −70 eV)	6.0% (−360 to −440 eV)	1.5% (−425 to −505 eV)

plane. As already noted by Schuch *et al.* [21], no correlations were observed between energy loss and vertical displacement [24] for a given recoil charge state within our resolution of ±50 eV. (Note that we observe only a projection of the angular distribution onto the y direction; see Sec. III above.) There is, however, an increase in scattering angle and energy loss with higher recoil charge states. Figures 8, 9, and 10 depict the vertical projection of the angular distribution for 10-MeV C^{6+} multiply ionizing Ne, Ar, and Kr. The lines represent the projectile scattering angle in coincidence with the recoil ion. Scattering angle differential cross sections for Ne have been reported earlier [21] and reasonable agreement with nCTMC calculations was found. We can see that for all

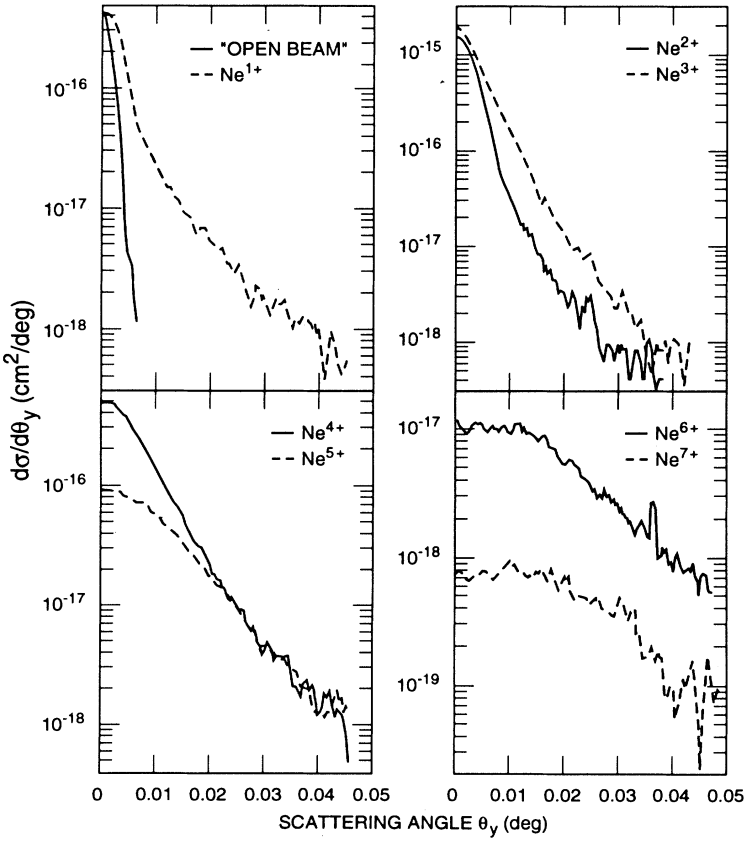

FIG. 12. Projection of angular distribution in the x-y plane for 10-MeV C^{6+}, which has undergone capture to C^{5+} in coincidence with Ne^{q+}

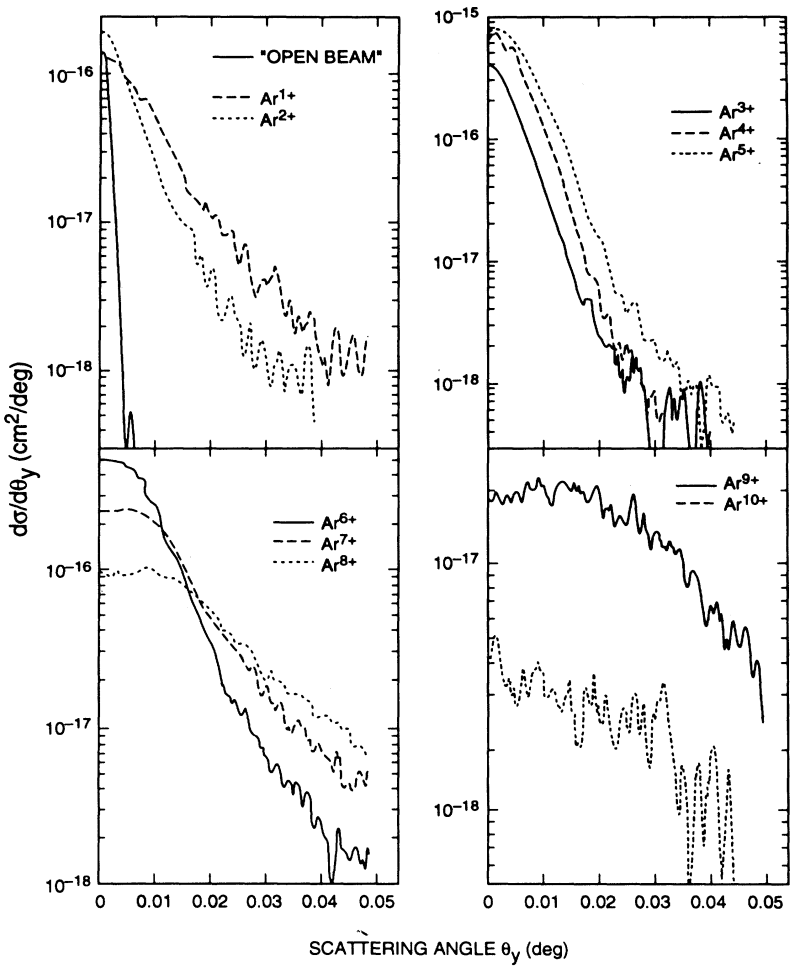

FIG. 13. Projection of angular distribution in the x-y plane for 10-MeV C^{6+}, which has undergone capture to C^{5+} in coincidence with Ar^{q+}.

targets, the mean scattering angle increases as we go to higher recoil-ion charge states. Furthermore, the scattering angle for a given recoil-ion charge state steadily decreases for higher Z targets, indicating that ionization is possible with increasingly larger impact parameters. This result is in accord with the observed decrease in energy loss per released electron with increasing target Z.

B. Capture

Because of the large dispersion of the spectrometer, the C^{5+} ions, which had captured an electron, and the C^{6+} ions that had not undergone collision did not strike the same detector. Hence, there was no zero energy-loss reference point and the absolute energy loss associated with single capture unaccompanied by ionization could not be determined. The relative projectile energy loss of 10-MeV C^{6+} in coincidence with single charge transfer versus the associated recoil charge state of different target gases is shown in Fig. 11. The energy loss for recoil charge-state 2 and higher is shown relative to recoil charge-state 1. The projectile energy loss for recoil charge-state 1 has been chosen arbitrarily to be 25 eV. Again, the projectile energy loss increases strongly with the number of target electrons ionized. The energy loss for all targets does not differ within the error bars for the first four recoil charge states. After that, the energy loss increases more than linearly and there is an apparent target-Z effect. The energy loss is smaller for increasing target Z. There is a steeper increase in energy loss with increasing recoil charge state than is found for the DI

TABLE IV. Projectile energy loss in eV for 7.5–25-MeV C^{6+} directly ionizing He and Ne. Energy loss is tabulated in reference to singly charged ions. Energy loss for A^{1+} is listed in parentheses where measured. *, not measured; and **, random coincidence rate does not permit an accurate energy-loss determination.

	7.5 MeV	10 MeV	20 MeV	25 MeV
		Ne		
1+	(220)	(280)	*	*
2+	530±60	280±60	156±50	147±50
3+	930±65	600±50	355±65	176±75
4+	1370±75	930±75	445±100	**
5+	1750±110	1220±70	**	**
6+	1820±130	1250±130	**	**
		He		
1+		(440)	*	*
2+		260±50	103±70	156±70

case. To get a qualitative understanding of this effect, we make the simplifying assumption that capture and ionization are independent processes. We now can attempt to compare the energy-loss data for capture plus multiple ionization with direct ionization. In the capture case, one electron is bound to the projectile; therefore, to treat the case for an equal number of electrons lost to the continuum, we have to compare charge state q with $q+1$ for the direct ionization case. The comparison shows [29] a marginally smaller energy loss for the transfer reaction for the first three charge states. After that, the charge exchanged projectiles show an increasingly larger energy loss per electron to the continuum than for ionization. This difference from direct ionizing collisions may be attributed to a recoil charge-state production that is dependent on initial to final n-state capture probabilities. Experiments by Konrad [30] and Justiniano, Konrad, and Schuch [31] for 115-MeV $S^{13+,14+,15+}$ impinging on Ne, Ar, and Kr targets demonstrated that when capture from inner shells occurs, the higher-recoil charge states are greatly increased. In Table III, we have estimated the n-state-dependent Oppenheimer-Brinkman-Kramers (OBK) capture cross sections [32,33] and Q value of the reaction. The Q value listed is calculated as the difference in binding energies of target and projectile minus the energy to accelerate the captured electron up to the projectile velocity. By including a change of the electron's kinetic energy we implicitly assume that capture occurs from the entire Compton profile of the target electrons. Negative energy values correspond to an energy loss of the projectile. By requiring a high-recoil charge state, the projectile will be less likely to capture from the most dominant channel. Instead, it will capture electrons as in the case of Argon, predominantly from $n=2$ and hence lose an additional energy of about 200 eV. These energy shifts are large enough to account for the observed nonlinear increase in energy loss.

The reported nCTMC calculations of energy loss shown in Fig. 11 are normalized to the data at Ne^{1+} to facilitate comparison. The absolute energy loss computed with nCTMC [26] for the Ne^{1+} is 760 eV, which agrees with the OBK approximation for the binding energy balance between target and projectile and the energy needed to accelerate the electron up to the projectile velocity. Overall, the nCTMC calculation can effectively reproduce the measured energy loss.

The scattering angles associated with capture to the projectile are larger than in the case of pure target ionization. Figures 12–14 show the scattering distribution of 10-MeV C^{6+} capturing and multiply ionizing Ne, Ar, and Kr. As in the case of direct ionization, the scattering angle for a fixed degree of target ionization decreases with

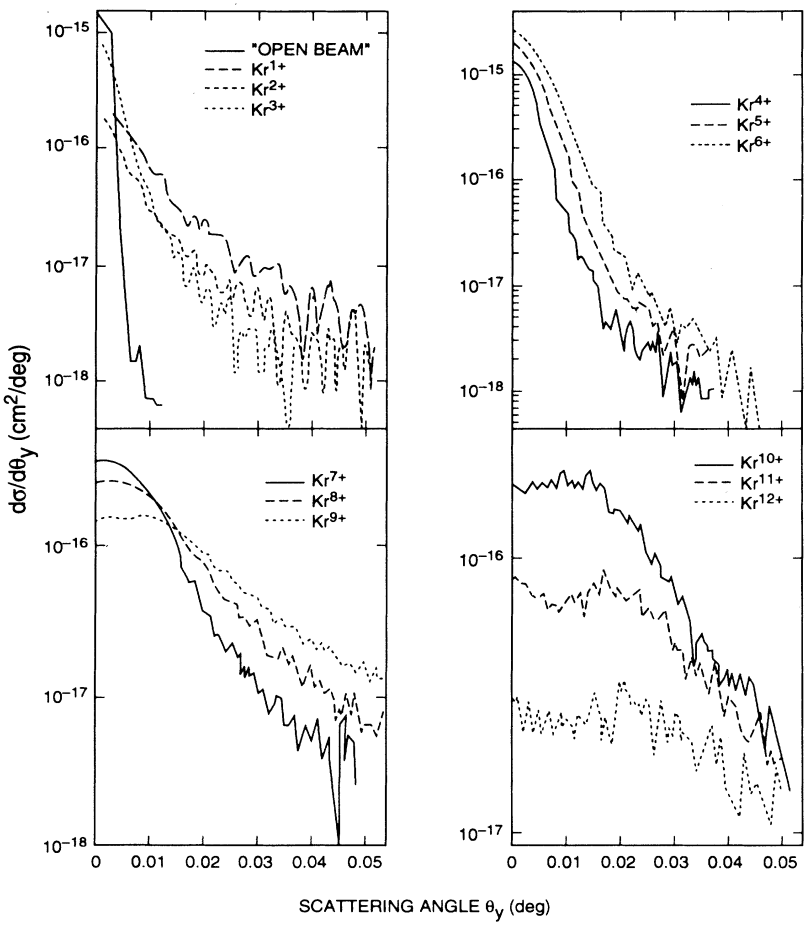

FIG. 14. Projection of angular distribution in the x-y plane for 10-MeV C^{6+}, which has undergone capture to C^{5+} in coincidence with Kr^{q+}.

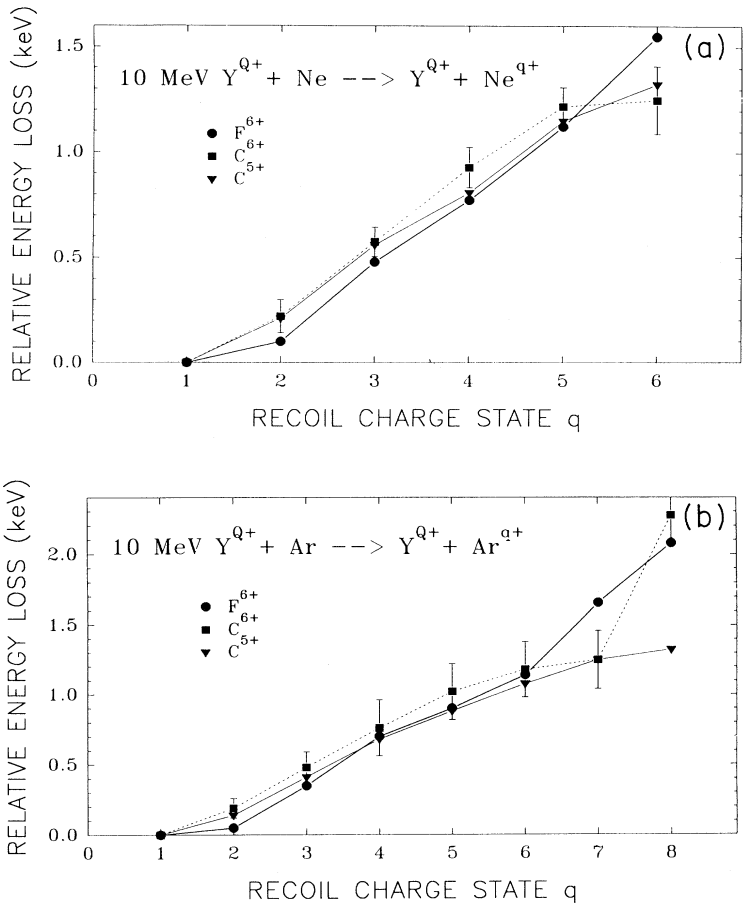

FIG. 15. Relative energy loss of F and C projectiles directly ionizing (a) Ne and (b) Ar, respectively.

larger atomic number of the target. This trend is again reflected in a decreased energy loss with increasing target Z. For very high-recoil charge states (in particular, Ne^{7+}, $Ar^{8+,9+}$, and $Kr^{10+,11+12+}$), a decrease in the differential cross section $d\sigma/d\theta_y$ is noticeable for small scattering angles, confirming that large impact parameters do not contribute significantly to the highly ionizing collisions.

C. Projectile energy and Z dependences

As the projectile energy increases from 7.5–25 MeV, the maximum transferable energy in a binary electron-projectile collision will increase. However, we find a decrease in energy loss with increasing C^{6+} ion energy. In Table IV, the C^{6+} energy loss in He and Ne collisions is listed for collision energies from 7.5–25 MeV, respectively. The absolute energy loss was not determined for 20- and 25-MeV projectiles, and the energy loss is reported with respect to singly charged recoil ions. Values in brackets give the energy loss for singly charged ions at collision energies of 7.5 and 10 MeV. The cross sections for collision energies of 20 and 25 MeV were too small to determine the energy loss for the higher-recoil charge states. The projectile scattering angle for a given recoil-ion charge state is also shown to decrease with increasing projectile energy. This reflects the fact that in a binary collision between an electron and an ion, the momentum transfer decreases with increasing velocity. The reduced energy loss is also in accordance with stopping power measurements which, for this energy range, show a reduction in stopping power with energy.

The dependence of the energy loss on projectile charge state has been measured for 10-MeV $C^{5+,6+}$ and F^{6+}. The $1s$ electron of C^{5+} can be considered passive because its ionization cross section is only about 0.1% of the target ionization cross section. Similarly, the effective charge for C^{6+} and F^{6+} can be considered equal for impact parameters where the projectile and target electron shells do not penetrate each other during the collision. The results are shown for direct ionization of Ne in Fig. 15(a) and for charge capture from Ar in Fig. 15(b), respectively. Within the margin of error, there are no significant differences observed. This result is in accord with measurements of stopping power made with totally stripped, one-electron and two-electron ions in crystal channels, where the charge state remains the same throughout the target [34]. There it was shown that the bound electrons screened with an efficacy of 90%. The difference between C^{5+} and C^{6+} is expected to be only 30%, i.e., within the error stated.

VI. CONCLUSION

In summary, we have observed a large projectile energy loss with the major part of the energy being

transferred to the ionized electrons. It had been shown that the average energy transferred per electron is largely independent of the recoil charge state produced. Comparison with model calculations such as SCA and *n*CTMC reveal the greatest discrepancies for the energy loss of low-recoil charge states. All model calculations used represent well the measured recoil charge-state distributions. This emphasizes the importance of highly differential measurements as a stringent test for the models used and a thorough understanding of the processes involved. For increasing target Z, a small decrease in the projectile energy loss was observed for a given recoil charge state. Residual target excitation can be neglected for the systems studied, hence the projectile energy-loss dependence on the target Z can be explained by the change in the energy transferred to the ionized electrons. In this work, the x displacement is a direct measure of the energy loss. The y displacement, however, is a projection of the scattering angle in the y-z plane onto the x-y plane, and the scattering angle is related to the impact parameter. We observe no change in x with increasing y. The implications from this result are that for a given ion charge state, there is a limited range of impact parameters involved and that the distribution in energy losses for this state is relatively narrow. To get a complete picture, it would be necessary to determine the energy distribution for each ionized electron in coincidence with the recoil charge state. This would address better the questions of how the large energy transfer to the electrons is shared between the ionized electrons and which ionization processes are dominant. In fact, it is hardly possible to measure the energy and momentum of each electron and ion in the collision. Frohne *et al.* [35] presented a method to measure the translational recoil momentum transfer in multiply ionizing collisions. By observing the recoil momentum and both the recoil and projectile charge states, it is possible to determine the total Q value, but *only* if all the electrons are bound to either the projectile or target. If this is the case, the recoil's momentum change directly reflects the projectile energy loss. Unfortunately, the comparison made by Frohne *et al.* between the recoil method and the energy-loss results using the technique described in this paper is not possible when some of the electrons are ionized. However, by using the information from both the projectile energy loss and the recoil momentum measurement, it is possible to determine directly the momentum carried off by the continuum electrons. As no detectable recoil momentum was observed for direct ionization, they concluded that almost all the momentum was transferred to the target electrons. This is in accordance with our findings, as stated earlier in this paper.

ACKNOWLEDGMENTS

This research was sponsored by the U.S. Department of Energy, Office of Basic Energy Sciences, Division of Chemical Sciences, under Contract No. DE-AC05-84OR21400, with Martin Marietta Energy Systems, Inc. The authors would like to thank R. E. Olson for providing *n*CTMC cross sections and energy-loss calculations prior to publication. Two of the authors (H.S. and R.S.) express their gratitude for the hospitality received at Oak Ridge National Laboratory.

[1] C. L. Cocke, Phys. Rev. **20**, 749 (1979).
[2] T. J. Gray, C. L. Cocke, and E. B. L. Justiniano, Phys. Rev. A **22**, 849 (1980).
[3] A. S. Schlachter, W. Groh, A. Müller, H. F. Beyer, R. Mann, and R. E. Olson, Phys. Rev. A **26**, 1373 (1982).
[4] J. H. McGuire and L. Weaver, Phys. Rev. A **16**, 41 (1977).
[5] J. Bang and J. M. Hansteen, Kgl. Dan. Vidensk. Selsk. Mat. Fys. Medd. **31**, 1 (1959).
[6] R. E. Olson, J. Phys. B **12**, 1843 (1979).
[7] G. Basbas, W. Brandt, and R. Laubert, Phys. Rev. A **17**, 667 (1978).
[8] A. Abrines and I. C. Percival, Proc. Phys. Soc. London **88**, 861 (9166); **88**, 873 (1966).
[9] R. E. Olson and A. Salop, Phys. Rev. A **16**, 531 (1977).
[10] A. Müller, B. Schuch, W. Groh, and E. Salzborn, Z. Phys. D **7**, 251 (1987).
[11] J. C. Levin, C. S. O, H. Cederquist, C. Biedermann, and I. Sellin, Phys. Rev. A **38**, R2674 (1988).
[12] O. Heber, G. Sampoll, B. B. Bandong, R. J. Maurer, E. Moler, R. L. Watson, I. Ben-Itzhak, J. L. Shinpaugh, J. M. Sanders, L. Hefner, and P. Richard, Phys. Rev. A **39**, 4898 (1989).
[13] I. Ben-Itzhak, T. J. Gray, J. C. Legg, and J. H. McGuire, Phys. Rev. A **37**, 3685 (1988).
[14] J. Ullrich, M. Horbatsch, V. Dangendorf, S. Kelbch, and H. Schmidt-Böcking, J. Phys. B **21**, 611 (1988).
[15] J. Ullrich, R. Olson, R. Dörner, V. Dangendorf, S. Kelbch, H. Berg, and H. Schmidt-Böcking, J. Phys. B **22**, 627 (1989).
[16] S. Kelbch, C. L. Cocke, S. Hagmann, M. Horbatsch, C. Kellbch, R. Koch, and H. Schmidt-Böcking, Phys. Lett. A **127**, 92 (1988).
[17] R. E. Olson, J. Ullrich, and H. Schmidt-Böcking, Phys. Rev. A **39**, 5572 (1989).
[18] G. Schiwietz, B. Skogvall, N. Stolterfoht, D. Schneider, V. Montemayor, and H. Platten, Nucl. Instrum. Methods Phys. Res. Sect. B **40**, 178 (1989).
[19] L. H. Andersen, P. Hvelplund, H. Knudsen, S. P. Møller, K. Eslener, K.-G. Resnfelt, and E. Uggerhoj, Phys. Rev. Lett. **57**, 2147 (1986).
[20] R. Dörner, J. Ullrich, H. Schmidt-Böcking, and R. E. Olson, Phys. Rev. Lett. **63**, 147 (1989).
[21] R. Schuch, H. Schöne, P. D. Miller, H. F. Krause, P. F. Dittner, and S. Datz, Phys. Rev. Lett. **60**, 925 (1988).
[22] J. Borggreen, B. Elbek, and Perch Nielsen, Nucl. Instrum. Methods **24**, 1 (1963).
[23] H. Schöne, Ph.D. dissertation, University of Heidelberg (1990).
[24] R. Schuch, S. Datz, P. F. Dittner, H. F. Krause, and P. D. Miller, Nucl. Instrum. Methods Phys. Res. Sect. A **262**, 6 (1987).
[25] R. D. Cowan, *The Theory of Atomic Structure and Spectra* (University of California Press, Berkeley, CA, 1981), p. 12.
[26] R. E. Olson (private communication).
[27] R. Schuch, L. Andersson, H. Schöne, and S. Datz, Nucl. Instrum. Methods Phys. Res. Sect. B **42**, 566 (1989).

[28] A. Russek and J. Meli, Physica **49**, 222 (1970).
[29] H. Schöne, R. Schuch, S. Datz, P. F. Dittner, J. P. Giese, H. F. Krause, M. Schulz, and Q. C. Kessle, Nucl. Instrum. Methods Phys. Res. Sect. B **40**, 141 (1989).
[30] J. Konrad, Ph.D. dissertation, University of Heidelberg (1986).
[31] E. Justiniano, J. Konrad, and R. Schuch, Nucl. Instrum Methods Phys. Res. Sect. B **40**, 132 (1989).
[32] J. R. Oppenheimer, Phys. Rev. **31**, 349 (1928).
[33] M. C. Brinkman and H. A. Kramers, Proc. Acad. Sci. Amst. **33**, 973 (1930).
[34] S. Datz, J. Gomez del Campo, P. F. Dittner, J. A. Biggerstaff, and P. D. Miller, Phys. Rev. Lett. **38**, 1145 (1977).
[35] V. Frohne, S. Cheng, R. Ali, M. Raphaelian, C. L. Cocke, and R. E. Olsen, Phys. Rev. Lett. **71**, 696 (1993).

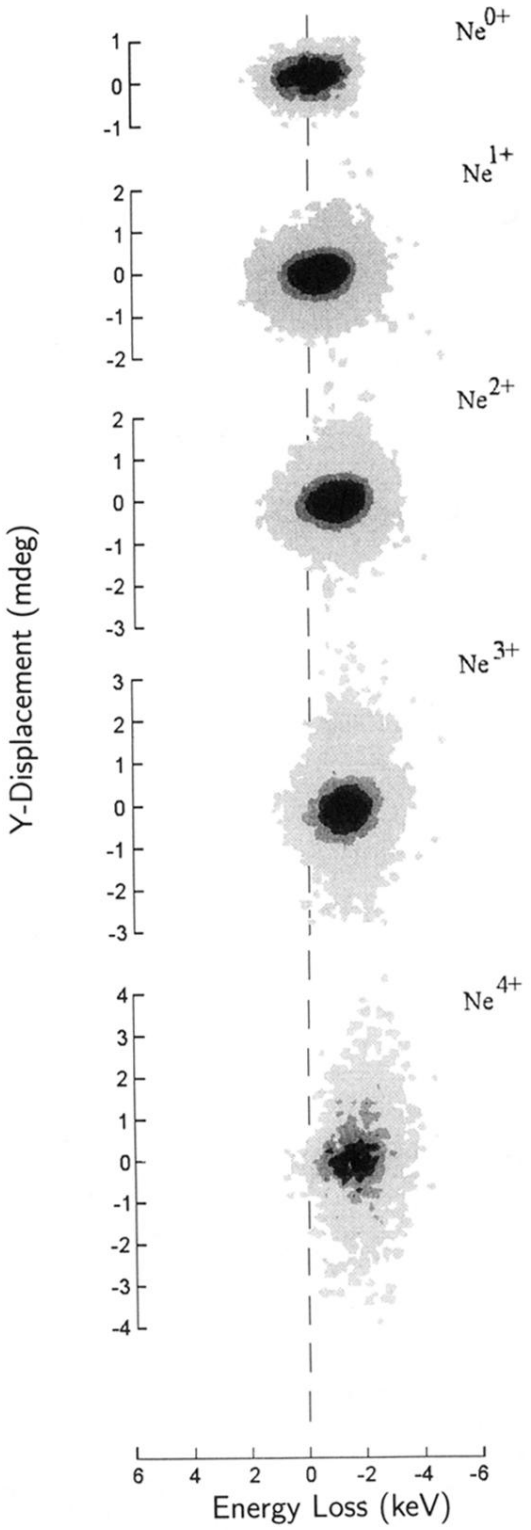

FIG. 4. Two-dimensional contour plot of projectile ion distributions in coincidence with recoil-ion charge state for direction ionization, i.e., $C^{6+}+Ne \rightarrow C^{6+}+Ne^{q+}+qe^{-}$. Ne^{0+} represents the projectile that did not ionize any target electrons.

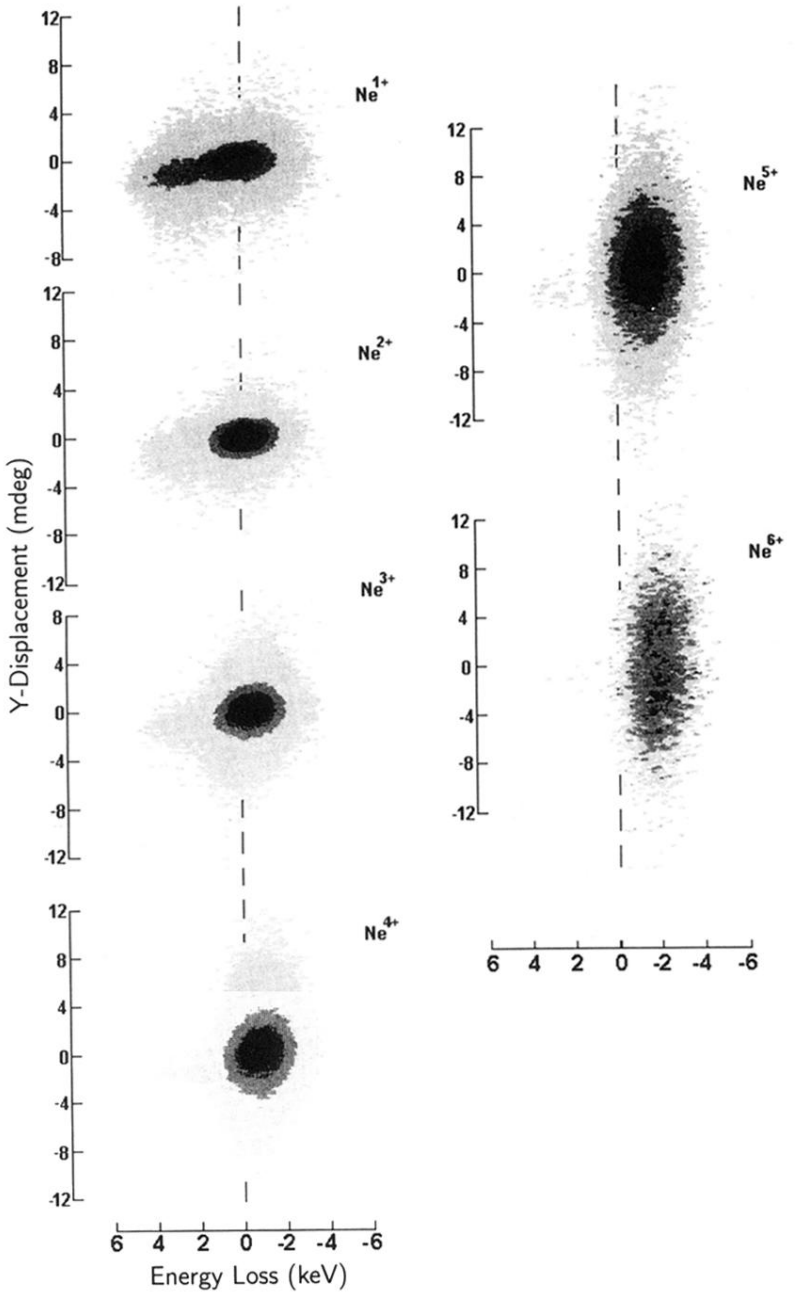

FIG. 5. Two-dimensional contour plot of projectile ion distributions in coincidence with recoil-ion charge state for collisions involving electron capture to the projectile, i.e., $C^{6+}+Ne \rightarrow C^{5+}+Ne^{q+}+(q-1)e^{-}$.